JMEPEG (2006) 15:535-539
DOI: 10.1361/105994906X136043

1059-9495/$19.00

Investigation of Thermal Formability of Aluminum Alloy 4032

G. Fang and P. Zeng

(Submitted July 9, 2005; in revised form December 19, 2005)

The deformation behavior of a 4032 aluminum alloy by hot compression has been investigated. It was found that the flow stress was strongly dependent on temperature as well as strain rate. The strain rate-sensitive coefficients were calculated at different temperatures. The experimental stress-strain data are fitted by means of the model earlier advanced by Sah et al. The Sellars-Tegart-Garofalo (STG) model is used to obtain activation energy values, which vary with the strain rate and strain.

Keywords aluminum alloy, constitutive equation, flow stress, hot deformation

1. Introduction

AA4032 is an aluminum-silicon alloy, the major alloying element of which is silicon, which can be added in sufficient quantities (up to 13.5 wt.%) to cause substantial wear resistance. For these reasons, it is mainly used in piston manufacturing. To study the formability of AA4032 alloy during hot deformation, accurate constitutive equations are needed to describe the deformation characteristics of the alloy. Some constitutive equations of other aluminum alloys were developed with dislocation models (Ref 1-3) and empirical models (Ref 4-6). The empirical models, which include stress, strain, strain rate, and temperature, are applied widely. The general form of constitutive equation is $\sigma = \sigma(T,\varepsilon,\dot{\varepsilon})$. Strain effects on flow stress are generally modeled with a hardening value of a power-like or exponent equation. Strain-rate effects are mostly modeled with a strain rate sensitivity parameter. Temperature dependence is often included in an Arrhenius term, which contains the apparent activation energy for the deformation process.

The aim of the present work was to investigate the effects of temperature and strain rate on the flow stress of an AA4032 alloy. The study focuses on the flow stress rather than the yield stress, because the test data of flow stress will be used in the processing simulation of the material by different forming technologies. Deformation temperature varied from 380 to 480 °C, and at each temperature a wide strain rate range of 0.01 to 10 has been covered. Compression testing has been used, and the flow stress data derived as a function of temperature, strain rate, and strain have been analyzed to gain an insight into the rate-controlling mechanism operating during hot deformation.

G. Fang and **P. Zeng**, Key Laboratory of Advanced Materials Processing Technology (AMPT), Department of Mechanical Engineering, Tsinghua University, Beijing 100084, China. Contact e-mail: fangg@tsinghua.edu.cn.

2. Experimental Procedures

The investigated alloy had the following chemical composition: Al = bal; Cr ≤ 0.1 wt.%; Cu = 0.5 to 1.3 wt.%; Fe ≤ 0.1 wt.%; Mg = 0.8 to 1.3 wt.%; Ni = 0.5 to 1.3 wt.%; Si = 11.0 to 13.5 wt.%; and Zn ≤ 0.25 wt.%. To determine the constitutive equation for the alloy, a number of stress-strain curves were used. Such curves were obtained with isothermal compression tests that were carried out in a Gleeble 1500D (Dynamic Systems Inc., Poestenkill, NY) thermomechanical testing machine. Cylinder samples with a height of 12 mm and a diameter of 8 mm were machined from the extruded rods. The graphite sheets were used at the end of samples as a lubricant during the tests.

To study the effects of temperature on the flow stress of an AA4032 alloy, the deformation temperatures were set at 380, 425, 450, and 480 °C. During tests, a thermocouple welded onto the sample surface was used to measure and control the temperature.

During every compression test, the strain rate was kept constant by the control of ram speed with computer software. Corresponding to every deformation temperature, four compression tests were carried out at strain rates of 0.01, 0.1, 1.0, and 10.0 s^{-1}.

All samples were compressed to a true strain of 0.8. The testing load-stroke curves were processed to obtain true stress-true strain curves generated by a standard program.

3. Experimental Results and Discussion

The flow stress data varying with strain were measured at four different temperatures and four different strain rates, as listed in Fig. 1. The curves show the flow stresses increase with strains and reach steady-state values.

3.1 Effects of Temperature and Strain Rate

In Fig. 1, we can find two types of stress-strain curves based on the varying stress values. At a lower strain rate (<1.0 s^{-1}), the stress-strain curves are of a steady-state type, although a subsequent rise in the flow stress occurred at a higher temperature (i.e., 480 °C). At higher strain rates, a peak occurs in yield stress and reaches a steady state at the high true stain.

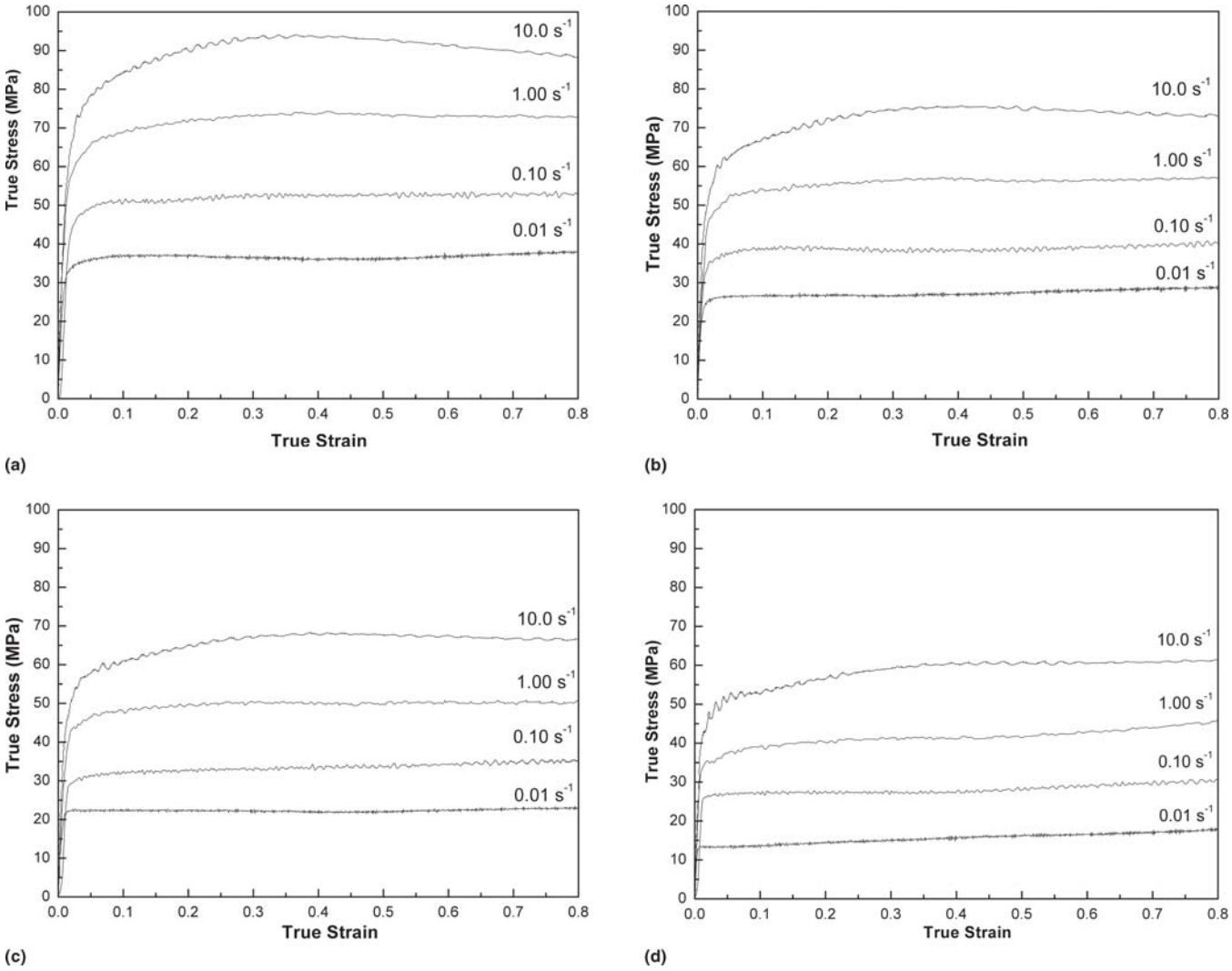

Fig. 1 True stress-true strain curves for the Al 4032 alloy at (a) 380 °C, (b) 425 °C, (c) 450 °C, and (d) 480 °C

The effects of temperature on the flow stress of the AA4032 alloy at different strain levels are described in Fig. 2. It can be seen that the flow stress at a given imposed strain rate depends on the temperature in a normal manner, decreasing with an increase of temperature. The effect of strain rate is brought out more clearly in Fig. 3, where it is noticed that the flow stress increases with strain rate at a given temperature. Similar behavior is observed at other strains. Therefore, the temperature and strain rate have important influence on the flow stress. With an increase of temperature, the flow stress decreases due to better plasticity (Fig. 2). To clearly describe the effect of strain rate, the curves in Fig. 3 are processed with $\ln(\sigma)$ versus $\ln(\dot{\varepsilon})$ and is shown in Fig. 4. The $\ln(\sigma)$ versus $\ln(\dot{\varepsilon})$ curve of the stress-strain rate is nearly linear, which indicates that there is a power relationship between the stress and strain rates. The strain rate sensitivity can be estimated from the slopes of these plots:

$$m = \frac{\Delta(\ln\sigma)}{\Delta(\ln\dot{\varepsilon})} \qquad \text{(Eq 1)}$$

where σ is the flow stress, $\dot{\varepsilon}$ is the strain rate, and m is the strain rate sensitivity. The m can be calculated by linear fitting of the stress-strain rate curves in Fig. 4. In Table 1, some m values corresponding to the true strain and temperature are listed. For the $\ln(\sigma)$ versus $\ln(\dot{\varepsilon})$, the curves at high temperature (i.e., 480 °C) are shown to be bilinear, and the m values are calculated from two values depending on the strain rate ($\dot{\varepsilon} < 1.0$ and $\dot{\varepsilon} \geq 1.0$). At temperatures of 380 to 450 °C, it was found that m values lay in the range 0.1193 to 0.1646, decreasing with increases in temperature, and the m values increase with true strain. But, at a temperature 480 °C the effects of strain rate on m are very important. With an increase in strain rate, the m value becomes small.

3.2 Constitutive Equations

At hot deformation, the aluminum alloy undergoes dynamic recovery and recrystallization. The flow stress curves show that a finite yield stress at the onset of plastic flow, and the stress tend to attain saturation at sufficiently large strains following a work-hardening transient. The strain dependence of flow stress during deformation in the general exponential saturation equation, as proposed by Sah et al. (Ref 7), is represented by:

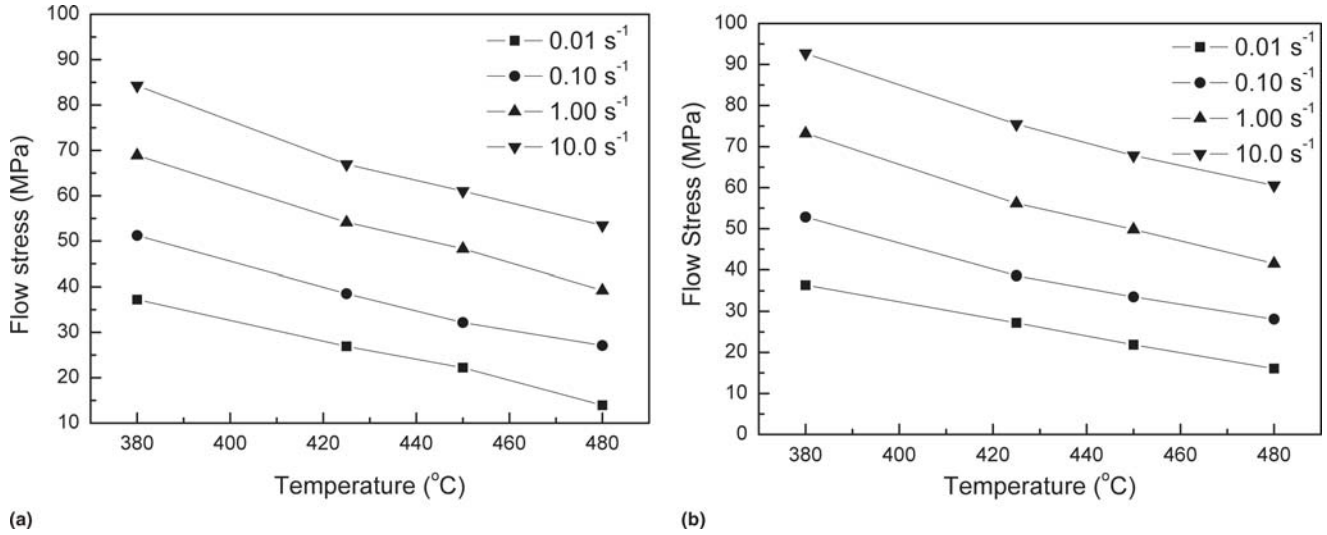

Fig. 2 Temperature and strain rate dependence of flow stress of Al 4032 alloy at true strain values of (a) 0.1 and (b) 0.5

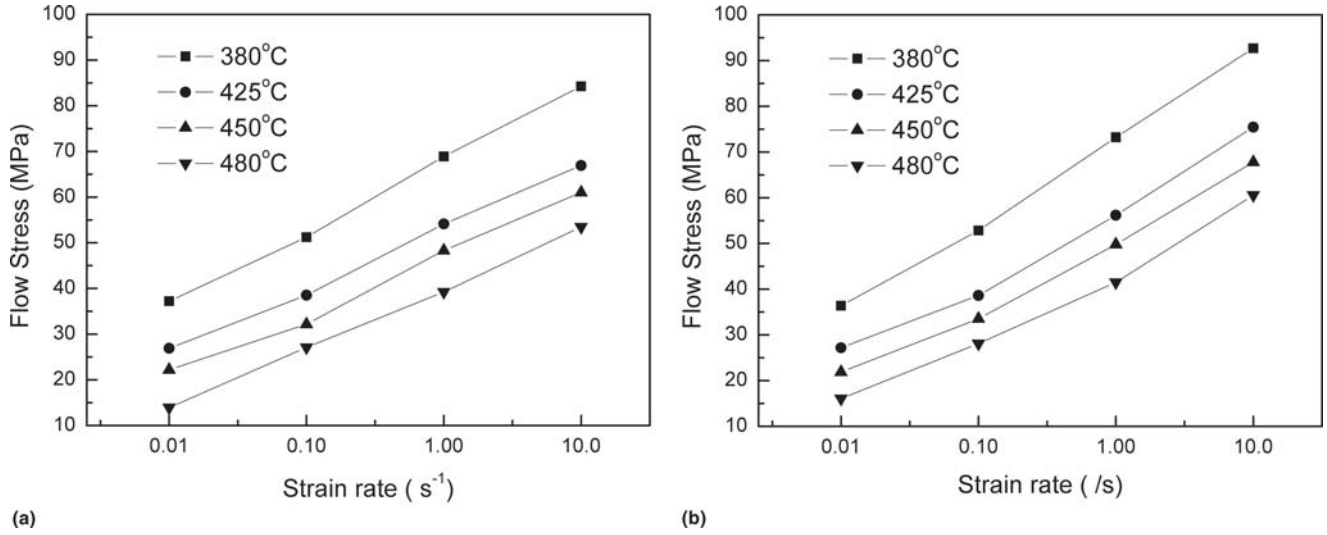

Fig. 3 Variation of flow stress of the Al 4032 alloy with strain rates at a true strain of (a) 0.1 and (b) 0.5

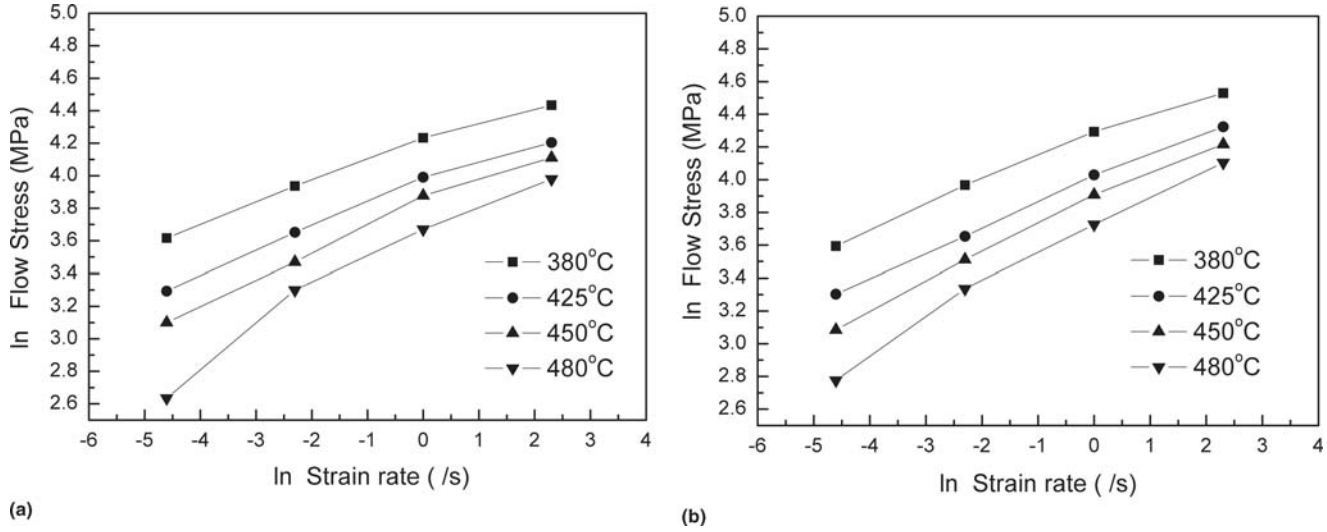

Fig. 4 Stress rate sensitivity of flow stress in the Al 4032 alloy at two true strain levels of (a) 0.1 and (b) 0.5

Table 1 Strain rate sensitivity *m* of Al 4032 alloy as a function of temperature and strain

	m at a true strain of	
Temperature, °C	0.1	0.5
380	0.1193	0.1361
425	0.1334	0.1493
450	0.1493	0.1646
480 ($\dot{\varepsilon} < 1.0$)	0.2887	0.2431
480 ($\dot{\varepsilon} \geq 1.0$)	0.1467	0.1666

$$\sigma = \sigma_0 + (\sigma_{SS} - \sigma_0)\left[1 - \exp\left(-\frac{\varepsilon}{\varepsilon_r}\right)\right]^{1/2} \quad \text{(Eq 2)}$$

where σ is the flow stress during deformation, σ_0 is the flow stress level at which plastic flow begins, σ_{ss} is the steady-state value of flow stress reached at high strains, ε is the strain during deformation, and ε_r is the relaxation or transient strain.

Table 2 lists some fitting coefficients of Eq 2 for the AA4032 alloy at a temperature of 400 °C. The comparison between experimental curves and fitting curves is shown in Fig. 5. These curves can describe material flow laws perfectly. It indicates that the model of Sah et al. (Ref 7) can be used to characterize both the flow stress and the work-hardening behavior under different deformation conditions. The three variables, that is, σ_0, σ_{ss}, and ε_r, rise with increases in the strain rate. It shows that the yield stress and the work-hardening rate of material are higher at a larger strain rate than ones at a smaller strain rate.

From Eq 2, it was found that the effects of temperature on stress cannot be included in constitutive relations. Some other constitutive equations for aluminum alloys were built to describe the temperature effects on the material flow (Ref 8, 9). The temperature dependence of the flow stress is often described by the classic Dorn-type Arrhenius equation (Ref 10), which contains the apparent activation energy for the deformation process:

$$\dot{\varepsilon} = A\sigma^n \exp\left(\frac{-Q}{kT}\right) \quad \text{(Eq 3)}$$

where A is a constant, n is a stress exponent (the reciprocal of m), Q is an activation energy of deformation, and k is the universal gas constant (8.31451 J/mol/K). When the strain rate and stress exponent are constants, Eq 3 can be expressed as:

$$\ln \sigma = \left(\frac{Q}{nk}\right)\frac{1}{T} + \frac{\ln \dot{\varepsilon} - \ln A}{n} \quad \text{(Eq 4)}$$

The curve of $\ln \sigma$ versus $(1/T)$ at a constant strain rate is plotted in Fig. 6, the slope of which (Q/nk) can been used for calculating Q (Table 3). Although the activation energy is fairly independent of strain rate and strain, the authors can observe some strain and strain rate dependence of activation energy. It was found that Q varies from ~169 kJ/mol to 325 kJ/mol. At a high strain rate ($\dot{\varepsilon} = 10.0\ s^{-1}$), an activation energy of ~170 KJ/mol can be obtained, which is close to the value calculated for self-diffusion in the aluminum alloy. But at a low strain rate ($\dot{\varepsilon} < 10\ s^{-1}$), the activation energy values become larger than those calculated at a high strain rate. The cause of the higher activation energy may be the higher silicon component and the lower solubility of Si and Mg in the AA4032 alloy than in other aluminum alloys.

Table 2 Fitting coefficients for Eq 2 for AA4032 (400 °C)

	Fitting coefficients		
Strain rate	σ_0	σ_{ss}	ε_r
0.01	24.839	27.501	0.062
0.10	25.354	38.901	0.028
1.00	41.984	56.613	0.096
10.0	42.842	74.672	0.107

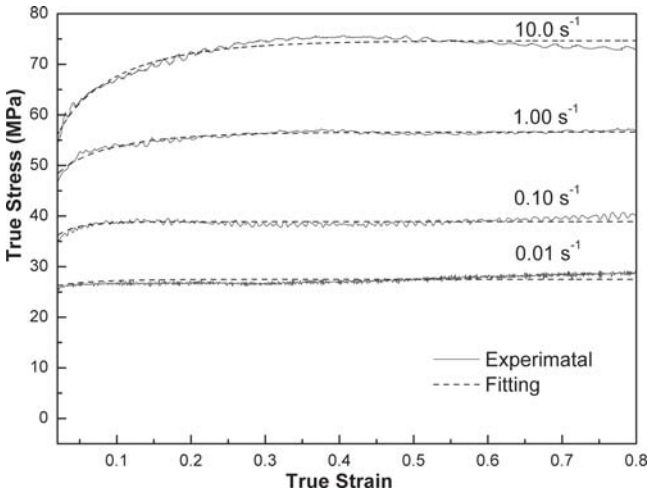

Fig. 5 Fitting curves of true stress-true strain for the Al 4032 alloy deformed at 400 °C

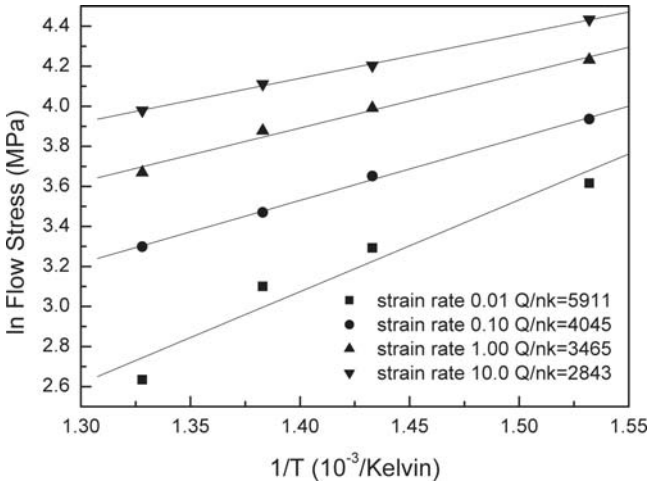

Fig. 6 Dependence relationship between flow stress and temperature

Figure 7 shows the microstructures of samples before and after compression. In these samples, there are primary aluminum solution dendrites and eutectic Al-Si, which have important influences on AA4032 deformation, distributed along the aluminum grain boundaries. After the compression, the aluminum solution dendrites underwent more deformation than the eutectic Al-Si phase and became finer than the primary samples.

Table 3 Calculated activation energy of deformation at the different conditions

	Activation energy Q, kJ/mol			
Strain	**$\dot{\varepsilon}$ = 0.01**	**$\dot{\varepsilon}$ = 0.10**	**$\dot{\varepsilon}$ = 1.00**	**$\dot{\varepsilon}$ = 10.0**
0.1	325	204	211	173
0.5	298	223	206	169

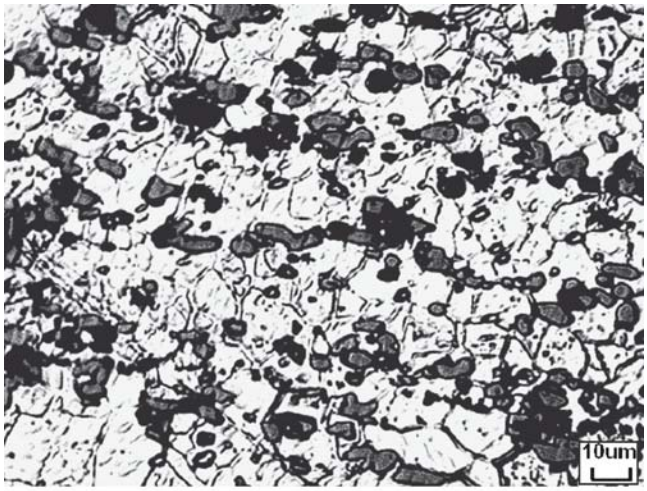

Fig. 7 Optical micrographs of the 4032 aluminum alloy (a) initially (before compression) and (b) after compression testing at 450 °C and strain rate 10 s^{-1}

4. Conclusions

The strain, strain rate, and temperature dependence of flow stress for the AA4032 alloy during deformation were analyzed with the compression experimental data. The constitutive equation model proposed by Sah et al. (Ref 7) is used to describe the strain dependence of the flow stress. The fitting curves of strain-stress agreed with the experimental data. From these curves and fitting variables, the strain rate dependence of flow stress can be investigated. To investigate the effects of temperature on flow stress and the activation energy, the classic Dorn-type Arrhenius equation is applied. It is shown that the apparent activation energy values obtained deviate from some values of pure aluminum and aluminum alloys in other literature. The higher silicon component and the lower solubility of Si and Mg may be the cause of the higher apparent activation energy values.

Acknowledgment

The authors gratefully acknowledge the support of National Natural Science Foundation of China (Grant No. 50205013).

References

1. N. Erik, Modelling of Work Hardening and Stress Saturation in FCC Metals, *Prog. Mater. Sci.,* 1997, **41,** p 129-193
2. Y. Estrin and H. Mecking, A Unified Phenomenological Description of Work-Hardening and Creep Based on One-Parameter Models, *Acta Metall.,* 1984, **32,** p 57-70
3. F. Barlat, M.V. Glazov, J.C. Brem, and D.J. Lege, Simple Model for Dislocation Behavior, Strain and Strain Rate Hardening Evolution in Deforming Aluminum Alloys, *Int. J. Plast.,* 2002, **18,** p 919-939
4. S. Spigarelli, E. Evangelista, and H.J. McQueen, Study of Hot Workability of a Heat Treated AA 6082 Aluminum Alloy, *Scripta Mater.,* 2003, **49,** p 179-183
5. H.J. McQueen, X. Xia, Y. Cui, B. Li, and B. Meng, Solution and Precipitation Effects on Hot Workability of 6201 Alloy, *Mater. Sci. Eng., A,* 2001, **319-321,** p 420-424
6. B. Verlinden, A. Suhadi, and L. Delaey, A Generalized Constitutive Equation for an aa6060 Aluminum Alloy, *Scripta Metall. Mater.,* 1993, **28,** p 1441-1446
7. J.P. Sah, G. Richardson, and C.M. Sellars, Recrysallization During Hot Deformation of Nickel, *J.Aust. Inst. Metall.,* 1969, **14,** p 292-297
8. J. van de Langkruis, W.H. Kool, and S. van der Zwaag, Assessment of Constitutive Equations in Modeling the Hot Deformability of Some Overaged Al-Mg-Si Alloys with Varying Solute Contents, *Mater. Sci. Eng., A,* 1999, **266,** p 135-145
9. P. Cavaliere, Hot and Warm Forming of 2618 Aluminum Alloy, *J. Light Metals,* 2002, **2,** p 247-252
10. H.J. McQueen, E. Fry, and J. Belling, Comparative Constitutive Constants for Hot Working of Al-4.4Mg-0.7Mn (AA5083), *J. Mater. Eng. Perform.,* 2001, **10,** p 164-172